

The Parkes quarter-Jansky flat-spectrum sample

2. New Optical Spectra and Redshift Measurements

I. M. Hook¹, P. A. Shaver², C. A. Jackson³, J. V. Wall¹, and K. I. Kellermann⁴

¹ Department of Physics, University of Oxford, Nuclear & Astrophysics Laboratory, Keble Road, Oxford, OX1 3RH, UK

² European Southern Observatory, Karl Schwarzschild Straße 2, D-85748 Garching b. München, Germany

³ Research School of Astronomy & Astrophysics, The Australian National University, Mount Stromlo Observatory, Canberra, Australia

⁴ National Radio Astronomy Observatory, 520 Edgemont Road, Charlottesville, VA 22903-2475, USA*

version November 20, 2018

Abstract. We present optical spectra and redshift measurements for 178 flat-spectrum objects from the Parkes quarter-Jansky flat-spectrum sample**. These spectra were obtained in order to compile a complete sample of quasars for use in a study of quasar evolution. We present a composite optical spectrum made from the subset of 109 quasars that have flux densities in the range $0.25\text{Jy} < S_{2.7\text{GHz}} < 0.5\text{Jy}$, and make a comparison with a composite for radio-quiet QSOs from the Large Bright Quasar Survey. Our large sample of radio-loud quasars allows us to strengthen previous reports that the Ly α and CIV emission lines have larger equivalent width in radio-loud quasars than radio-quiet QSOs to greater than the 3σ level. However we see no significant difference in the equivalent widths of CIII] or MgII. We also show that the flux decrements across the Lyman- α line (D_A) measured from these spectra show the same trend with redshift as for optically selected QSOs.

Key words. quasars:general radio

1. Introduction

This is the second paper in a series of three describing the results of a program to search for high-redshift quasars and study the evolution of the flat-spectrum radio-loud quasar population. The first paper (Paper 1, Jackson et al. 2002) set out the sample, discussing its selection and the identification and re-confirmation programme to determine the optical counterparts to the radio sources. This paper, Paper 2, presents new spectroscopic observations and redshift determinations. Paper 3 (Wall et al. 2002) considers the quasar space distribution, the luminosity function and its epoch dependence. Because the sample is radio selected, the completeness of the sample is unaffected by obscuration from dust. An earlier version of this sample was used by Shaver et al. (1996b) to show that

the space density of quasars declines at redshifts greater than 3.

In addition to the primary goal of this work (the study of quasar evolution), the sample can be used for several other statistical studies. It has provided the basis for a study of damped Lyman- α absorption systems along the lines of sight to the quasars (Ellison et al. 2001, 2002). In this paper we also consider some properties of the quasar spectra themselves, in particular the equivalent width distributions of the emission lines, and the flux decrement across the Lyman- α line at high redshift.

2. Definition of the spectroscopic sample

We have defined a sample of flat-spectrum radio sources from the PKSCAT90 catalogue (Wright & Otrupceck 1990) as described in Jackson et al. (2002). The sample of 878 sources was selected based on the following criteria: $\alpha_{2.7\text{GHz}}^{5.0\text{GHz}} > -0.4$, where $S \propto \nu^\alpha$, $-80^\circ < \delta < +2.5^\circ$, $|b| \geq 10^\circ$. The optical identification procedure, including new radio positions that were obtained as part of this study, is described in Jackson et al. (2002) and a full set of finding charts is given there. The majority of identifications were made using COSMOS scans of UKST B_J

Send offprint requests to: I. M. Hook e-mail: imh@astro.ox.ac.uk

* The National Radio Astronomy Observatory is operated by Associated Universities Inc. under a cooperative agreement with the National Science Foundation.

** Table A1 is also available in electronic form at the CDS via anonymous ftp to cdsarc.u-strasbg.fr (130.79.128.5) or via <http://cdsweb.u-strasbg.fr/cgi-bin/qcat?J/A+A/>

plates, and CCD identifications were obtained for those sources not identified on the plates. We refer to this sample as the Parkes quarter-Jansky flat-spectrum sample.

Since the primary aim of this project was to study the evolution of the quasar population using a complete sample, we then selected for spectroscopic follow up all those stellar sources (as determined from COSMOS or CCD identifications) with $S_{2.7\text{GHz}} \geq 0.25\text{Jy}$ in the zone north of -45° that did not have previous redshift measurements in the literature. In addition, a few sources south of declination -45° were also observed and their spectra are included in this paper, although the sample was not intended to be complete in that region.

3. Spectroscopic Observations

The spectroscopic observations were carried out at the ESO 3.6m at La Silla, Chile during observing runs in November 1993, May 1994, October 1994, April 1995, October 1995, May 1997 and October 1997. Observations were made of a total of 178 sources, the majority during the last two of these runs. Low resolution spectra were obtained using the EFOSC spectrograph with a $1.5''$ slit width. Most sources were observed at a sky position angle of 270° , i.e. not necessarily at the parallactic angle. In most cases the B300 grism (wavelength range $3750\text{--}6950\text{\AA}$, dispersion 6.35\AA per pixel) was used, but a few sources were observed with the R300 grism (wavelength range $6000\text{--}9910\text{\AA}$, dispersion 7.7\AA per pixel) either because the object was clearly red based on CCD identifications, or because the blue spectrum was ambiguous.

4. Results

As a result of the spectroscopic observations described above, the Parkes quarter-Jansky flat-spectrum sample has highly complete redshift information (see Jackson et al. 2002). In summary, there are 677 objects classified as quasars or BLs in the original sample of 878. A total of 174 of the objects classified as 'Q' (and none of the BLs) do not have spectroscopic confirmation. Note that in the analysis of the quasar space density in Paper 3, only the near-complete sub-sample with $\delta > -40$ deg is considered.

Of the 178 objects that we observed, 126 show strong, broad emission lines and were therefore classified as quasars. 37 objects showed featureless spectra or very weak lines on a strong continuum, and we classified these as BL Lac objects. The remaining 15 objects were classified as galaxies based on the presence of galaxy absorption lines, narrow emission lines or a strong 4000\AA break.

Mean redshifts were calculated from the emission lines (or absorption lines in a few cases). The rest frame wavelengths used for the quasar emission lines were those given in Tytler & Fan (1992), which have been corrected for small ($\sim 0.1\%$) systematic shifts between UV emission lines and the true systemic velocity. Since the Ly- α line is usually affected by Ly- α forest absorption it was not used

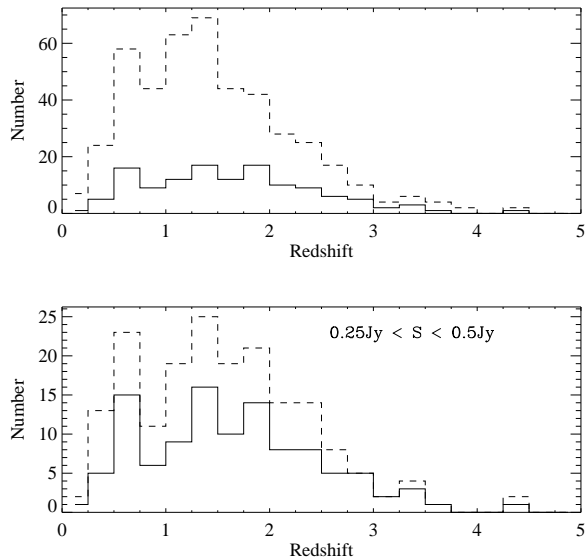


Fig. 2. Upper panel: Redshift histogram for all 449 quasars in the Parkes quarter-Jansky flat-spectrum sample (dashed line) and for the 126 new quasar spectra presented in this paper (solid line). Lower panel: As above but for sources with $0.25\text{Jy} \leq S < 0.5\text{Jy}$ (183 and 109 sources respectively).

to calculate the redshift unless there were no other clean lines in the spectrum.

The new spectra are plotted in Figure 1 and the redshifts are given in Table A.1. The redshift distribution for the new quasar spectra is shown in Figure 2. The flux density distribution for these objects is also plotted as a function of redshift in Figure 3.

The vast majority (109 from 126) of the quasars for which we have obtained spectra have flux densities in the range $0.25\text{Jy} < S_{2.7} < 0.5\text{Jy}$ (almost all sources stronger than this had redshifts from the literature). A K-S test shows that the distribution of these 109 new quasar redshifts is indistinguishable from that of all quasars in the Parkes quarter-Jansky flat-spectrum sample with $0.25\text{Jy} < S_{2.7} < 0.5\text{Jy}$. In the remainder of this paper we take this sample of 109 new quasar spectra as representative of the Parkes quarter-Jansky flat-spectrum quasar sample in this flux range, and we term this sample the PKS 0.25-0.5Jy sample.

4.1. Notes on Individual Objects

B0039–407 Iovino, Clowes & Shaver (1996) estimated the redshift as $z = 2.37$ from an objective prism measurement. We now measure $z = 2.478$.

B0138–097 Stocke & Rector (1997) give $z = 0.733$ for this BL source. Despite high signal-to-noise in the range $4000 - 7000\text{\AA}$, our spectrum does not confirm their MgII emission-line redshift of $z = 0.733$. We classify this source as a BL with undetermined redshift.

B0357–264 Drinkwater et al. (1997) give “ $z=1.47?$ ” for this source. Their spectrum does not show any strong

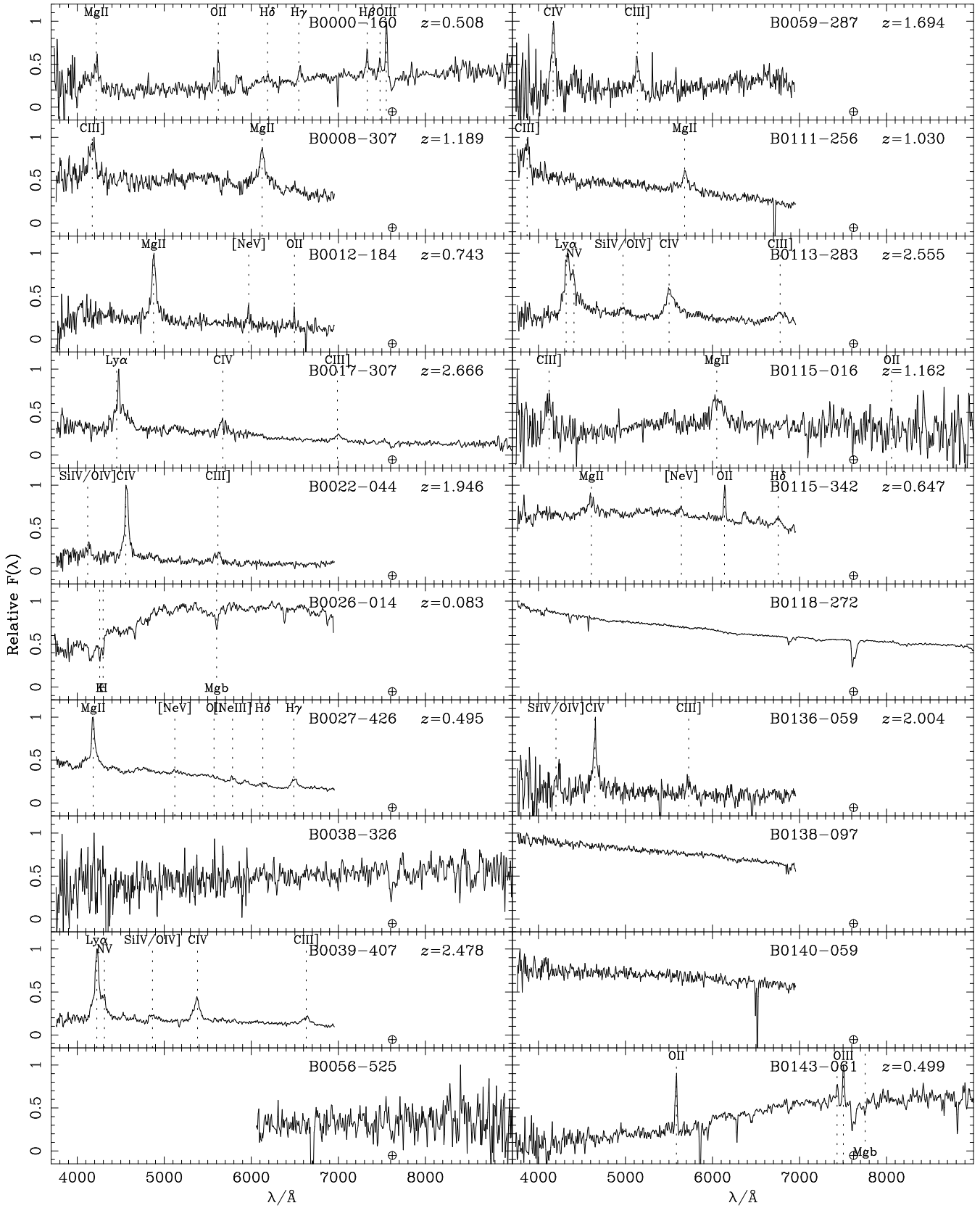


Fig. 1. New optical spectra for the Parkes quarter-Jansky flat-spectrum sample. The spectra have been scaled to have a maximum flux value of 1.0. The dotted vertical lines show the expected positions of spectral features at the measured mean redshift (not the measured wavelengths of the individual features). An asterisk after the redshift indicates an uncertain redshift. The earth symbol at $\sim 7600\text{\AA}$ indicates the position of the atmospheric absorption feature (the A-band).

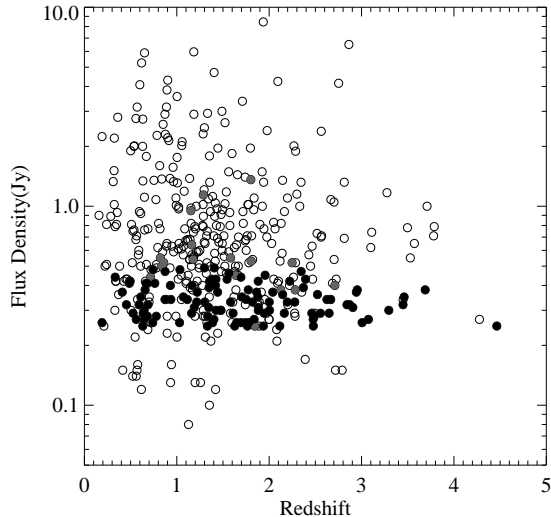


Fig. 3. Flux density vs Redshift for all quasars in the Parkes quarter-Jansky flat-spectrum sample (open circles). Quasars with new redshifts presented in this paper are plotted as filled circles: black circles for those used to make the composite, grey for the others.

features and it is not clear from their paper which features this redshift is based on. Our spectrum covers a similar wavelength range to that of the Drinkwater et al. spectrum but does not show sufficient features to measure a redshift. We therefore classify this source as a BL.

B0646–306 Veron-Cetty & Veron (1993) give $z=0.455$ for this object whereas we find $z = 1.153$. It is likely that the previous redshift determination was the result of misidentifying the CIII] line at $\sim 4100\text{\AA}$ with MgII.

B1136–156 The emission lines of CIV and Ly α are affected by absorption.

B1251–407 The previously published redshift of 4.458 (Shaver et al 1996a) was derived using different assumptions for the rest-frame wavelengths of the emission-lines. Using values corrected for systematic shifts (Tytler & Fan 1992) we derive a redshift of 4.464.

B2303–656 PKSCAT90 lists this object at a redshift of $z = 0.47$. Our spectrum, which starts at 6000\AA , does not show any clear features to confirm this.

B2224+006 The emission lines of CIV and Ly α are affected by absorption.

5. A Composite radio-selected QSO spectrum

5.1. Method for producing the composite spectrum

We have derived a composite spectrum from 109 of the quasar spectra shown in Figure 1 (i.e. those that lie in the PKS 0.25-0.5Jy sample) with the aim of comparing emission line strengths for radio and optically selected QSOs.

The B300 spectra were clipped to cover $3750 < \lambda < 6830\text{\AA}$ and those spectra taken with the R300 grism were clipped to $\lambda < 9300\text{\AA}$. The region from $7595 - 7645\text{\AA}$ in the R300 spectra, which is strongly affected by the sky absorption feature (A-band), was cut out of the spectra.

The spectra were then sorted by redshift, shifted to the rest frame and interpolated onto a common rest-frame wavelength grid. The composite was built up iteratively by including one more spectrum at each iteration. A scale factor was calculated for each spectrum by normalising it to the current composite (since the spectra were sorted in redshift, there is a large region of overlap in the rest frame between each new spectrum and the most recent iteration of the composite). Each iteration of the composite was formed by adding all the contributing points at that wavelength, scaled by the appropriate scale factor for that spectrum, and divided by sum of scale factors. Thus each spectrum has an equal weight in the composite. Figure 4 shows the number of spectra contributing to each rest wavelength bin.

Figure 5 shows the comparison of the PKS 0.25-0.5Jy composite with that for radio-quiet QSOs from the Large Bright Quasar Survey (LBQS; Hewett, Folz & Chaffee 1995 and references therein). This second composite was compiled and provided by P. Francis (private communication) and is similar to the radio-quiet composite presented by Francis, Hooper & Impey (1993) but has been updated to include a factor ~ 3 more QSOs, having made use of radio information from the FIRST survey (Becker, White & Helfand 1995) to distinguish between radio-loud and radio quiet QSOs in the LBQS. We refer to this new composite as the “LBQS radio-quiet composite.”

The continua of the two composites were found to have somewhat different slopes, the PKS 0.25-0.5Jy composite having a redder UV/optical continuum spectral index of $\alpha = -1.0$ compared to $\alpha = -0.32$ for the LBQS composite ($F(\nu) \propto \nu^\alpha$). However this may be at least in part an artefact caused by several systematic effects, as described in Francis et al. (1991). For example, the individual spectra that make up the PKS 0.25-0.5Jy composite were taken with a fairly narrow slit (typically $1.5''$ wide) and therefore flux may be lost at the ends of the spectra due to atmospheric dispersion. No attempt was made to correct for this. Because the composite was built up by including spectra in redshift sequence, these relative flux calibration errors may have the effect of producing a gradual gradient in the overall spectral shape of the composite.

For the purposes of plotting the two composites together, both were normalised by low-order polynomial fits to their continua (avoiding regions with strong lines for the continuum fit). There are some clear qualitative differences between the composite spectra shown in Figure 5. The main differences are that the Ly- α (1216\AA) and CIV(1549\AA) lines are stronger in the PKS 0.25-0.5Jy composite. Below we make a quantitative comparison of the emission line strengths relative to the local continuum.

5.2. Rest-frame equivalent width measurements

We have measured the rest-frame equivalent width (EW) of emission lines from the PKS 0.25-0.5Jy composite (Figure 5) and from an electronic version of the LBQS

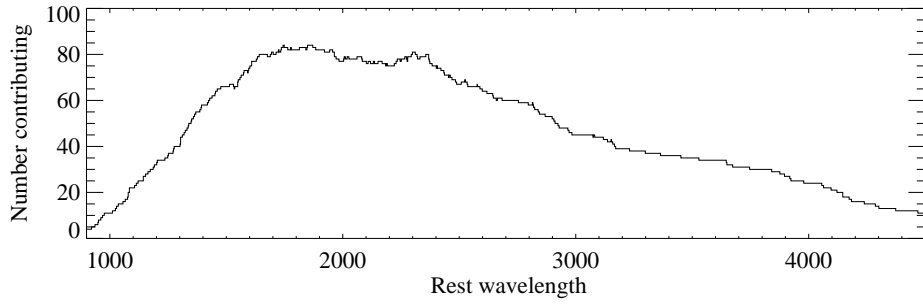


Fig. 4. The number of spectra contributing to the PKS 0.25-0.5Jy composite as a function of wavelength.

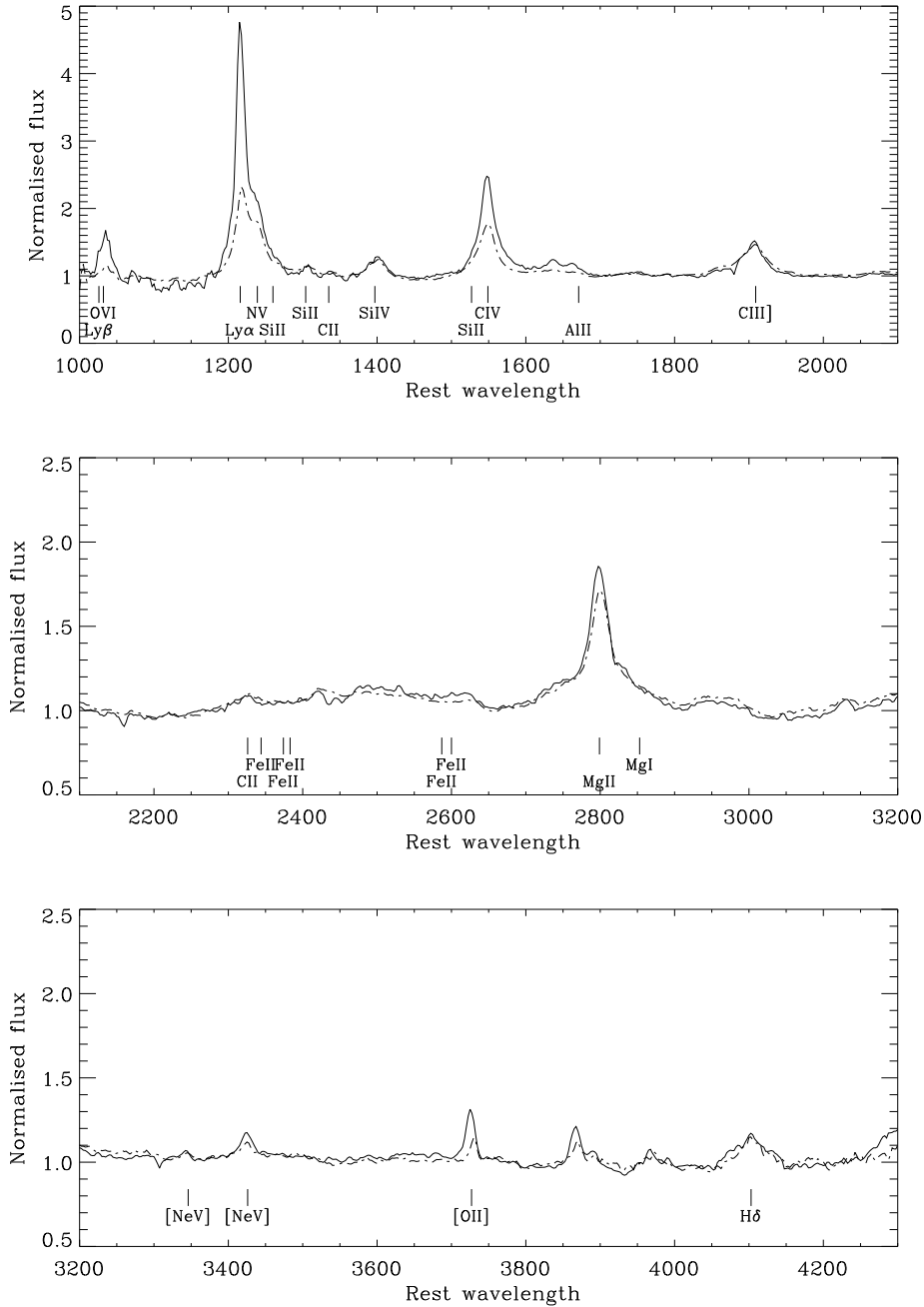


Fig. 5. Comparison of composite spectra for radio-loud and radio-quiet QSOs. The dashed line shows the LBQS radio-quiet composite. The solid line shows the PKS 0.25-0.5Jy (radio loud) quasar composite described in the text. Both composites have been normalised by their continua.

radio-quiet composite. This was done following the algorithm in Francis (1993) but using slightly different continuum and line wavelength ranges. The wavelength regions used were as follows: Ly α line 1216 – 1230Å (i.e. the red side of the line only, since the blue side is affected by Ly α absorption); Ly α continuum 1275 – 1295Å and 1440 – 1480Å; CIV line 1480 – 1590Å; CIV continuum 1450 – 1480Å and 1680 – 1700Å; CIII] line 1850 – 1940Å; CIII] continuum 1770 – 1820Å and 1970 – 2030Å; Fe II line complex 2300 – 2600Å; FeII continuum 2230 – 2260Å and 2650 – 2670Å; MgII line 2680 – 2900Å; MgII continuum 2640 – 2670Å and 3010 – 3060Å.

The ratios of the EWs are given in Table 1. For the PKS 0.25-0.5Jy sample we also measured the EWs of the lines from the individual spectra, and their distributions are shown in Figure 6. These distributions were used to estimate the dispersion of EW measurements. The mean deviation from the median, divided by \sqrt{N} (where N is the number of measurements of that line) was taken as an estimate of the uncertainty of the EW measured from the composite. For the LBQS composite the uncertainty in the EW measurements was derived using the mean and uncertainties given in Francis, Hooper & Impey (1993). Since those values correspond to a previous version of their LBQS radio-quiet composite, we have scaled the uncertainties by the inverse square root of the relative numbers of QSOs contributing to each line (which typically reduces the uncertainty by a factor ~ 2). The fractional uncertainty in the EW ratio was taken as the quadratic sum of the fractional uncertainties determined above.

Table 1 and Figure 6 show that the Ly α and CIV lines are significantly stronger in the PKS 0.25-0.5Jy sample than in the LBQS radio-quiet sample at greater than the 3σ level. This difference is unlikely to be a result of the Baldwin effect since the optical magnitude distribution of the LBQS, $m_{B_j} \leq 18.85$, and the redshift distribution (Hewett, Foltz & Chaffee 1995) are similar to those of the sample of quasars used to make our PKS 0.25-0.5Jy composite (see solid lines in Figures 2 and 7).

Previous authors have compared EW distributions of radio-loud and radio-quiet QSOs but found no significant differences (e.g. Steidel & Sargent 1991, Corbin 1992). However, as pointed out by Francis, Hooper & Impey (1993), this is generally because of small sample sizes and in fact these studies are consistent with the measurements of Francis, Hooper & Impey (1993) and with those in this paper to within 1σ . The more recent measurement of the CIV equivalent width ratio from Corbin & Francis (1994) of 1.21 ± 0.21 is also consistent with our work, although our measurements have lower uncertainties than these samples individually or combined.

The MgII line, CIII] line and the region dominated by iron lines (FeII) around 2400Å-2600Å do not show significant differences in equivalent width distribution between the PKS radio-loud and LBQS radio-quiet samples, in agreement with Francis, Hooper & Impey (1993).

We have also carried out a similar comparison using the combined LBQS composite of Francis et al. (1991),

which contains a small fraction ($\sim 10\%$) of radio-loud quasars. As would be expected the results were very similar to those shown in Table 1 since the combined LBQS composite is dominated by radio-quiet QSOs. When considering the ratios of EWs relative to the PKS 0.25-0.5Jy sample, as in column (c) of Table 1, only the ratio of Ly α EWs changed by more than 1σ . Using the combined composite the ratio was 2.12 ± 0.17 compared to 2.73 ± 0.19 .

Although the optical magnitudes of the PKS 0.25-0.5Jy sample and the LBQS sample are similar, the PKS sample is radio-selected and hence contains more extreme radio-loud objects than the radio-loud LBQS sub-sample in Francis, Hooper & Impey (1993). Almost all the LBQS sample members, including the radio-loud quasars, have radio flux densities well below the 0.25Jy flux limit of our sample (Hooper et al. 1995). As a result we might expect to see more pronounced differences between the PKS 0.25-0.5Jy composite spectrum and the LBQS radio-quiet composite than were seen between the radio-loud and radio quiet subsets of the LBQS sample. However we in fact find very similar ratios of EWs as were found by Francis, Hooper & Impey (1993) for all the lines considered except Ly α , which appears to be significantly stronger in the PKS 0.25-0.5Jy sample.

Brotherton et al. (2001) saw no significant difference in the Ly α line (or indeed any of the UV lines that we have studied) when they considered composite spectra of radio-loud and radio-quiet objects from the FIRST Bright Quasar Survey (FBQS). That sample is radio-selected but the faint flux density limit ($S_{1.4\text{GHz}} \sim 1\text{mJy}$) and bright optical limit ($E < 17.8$) means it is still sensitive to quasars that are formally radio-quiet, although as they point out, the extreme radio-quiet and “radio-silent” QSOs are not represented. It is possible that their result, that of Francis, Hooper & Impey (1993) and our result represent a trend of Ly α EW becoming progressively stronger with increased radio loudness. However, as Brotherton et al. (2001) also point out, their radio-quiet sub-sample has rather limited statistics - only ~ 12 quasars contribute to the Ly α line in their radio-quiet composite. Because of the difference in optical magnitude distributions of the FBQS and our sample, and hence the possible complication of the Baldwin effect, we have not carried out a detailed comparison with the FBQS composites.

We also note that the EWs of Ly α and CIV in classical radio galaxies are comparable but somewhat stronger than those found for the PKS 0.25-0.5Jy sample: values of EW=919Å for Ly α and 74Å for CIV are reported by McCarthy (1993), measured from a composite of high-redshift 3CR and 1Jy class radio galaxies. This, along with the appearance of HeIII1640 and stronger forbidden lines (see Figure 5), puts the PKS 0.25-0.5Jy sources on a smooth trend from radio-quiet to flat-spectrum quasar to steep-spectrum quasar to radio galaxy. This trend, at least among radio-loud quasars, has been interpreted by previous authors in the context of unified schemes of AGN. For example Baker & Hunstead (1995) found that the EW of narrow lines in radio-loud quasars from the Molonglo

Table 1. Rest-frame equivalent widths measured from our data compared with measurements from the literature. Column (a) gives the number of QSOs contributing to the statistics for our PKS 0.25-0.5Jy sample. Column (b) gives the median of the EW distributions from our PKS 0.25-0.5Jy sample. Column (c) lists the ratio of EW measurements determined from the PKS 0.25-0.5Jy composite and the LBQS Radio-quiet composite. The uncertainty in this estimate is derived from the distribution of EW measurements from the individual spectra that make up each composite (see text). Column (d) lists the ratio of EW measurements for radio-loud and radio-quiet subsets of the LBQS sample from Francis, Hooper & Impey (1993).

Line	(a)	(b)	(c) Composite Ratio	(d)
	N (PKS 0.25-0.5Jy)	Median EW (Å) (PKS 0.25-0.5Jy)	EW(PKS 0.25-0.5Jy) /EW(LBQS RQ)	EW(loud)/EW(quiet) Francis, Hooper & Impey (1993)
Ly α	30	21.3 ± 1.3	2.73 ± 0.19	1.56 ± 0.34
CIV	49	51.8 ± 3.1	1.50 ± 0.11	1.47 ± 0.24
CIII]	57	17.6 ± 1.6	0.86 ± 0.08	1.00 ± 0.11
FeII	36	25.5 ± 2.5	0.85 ± 0.10	1.06 ± 0.23
MgII	36	50.3 ± 7.6	1.15 ± 0.18	0.96 ± 0.12

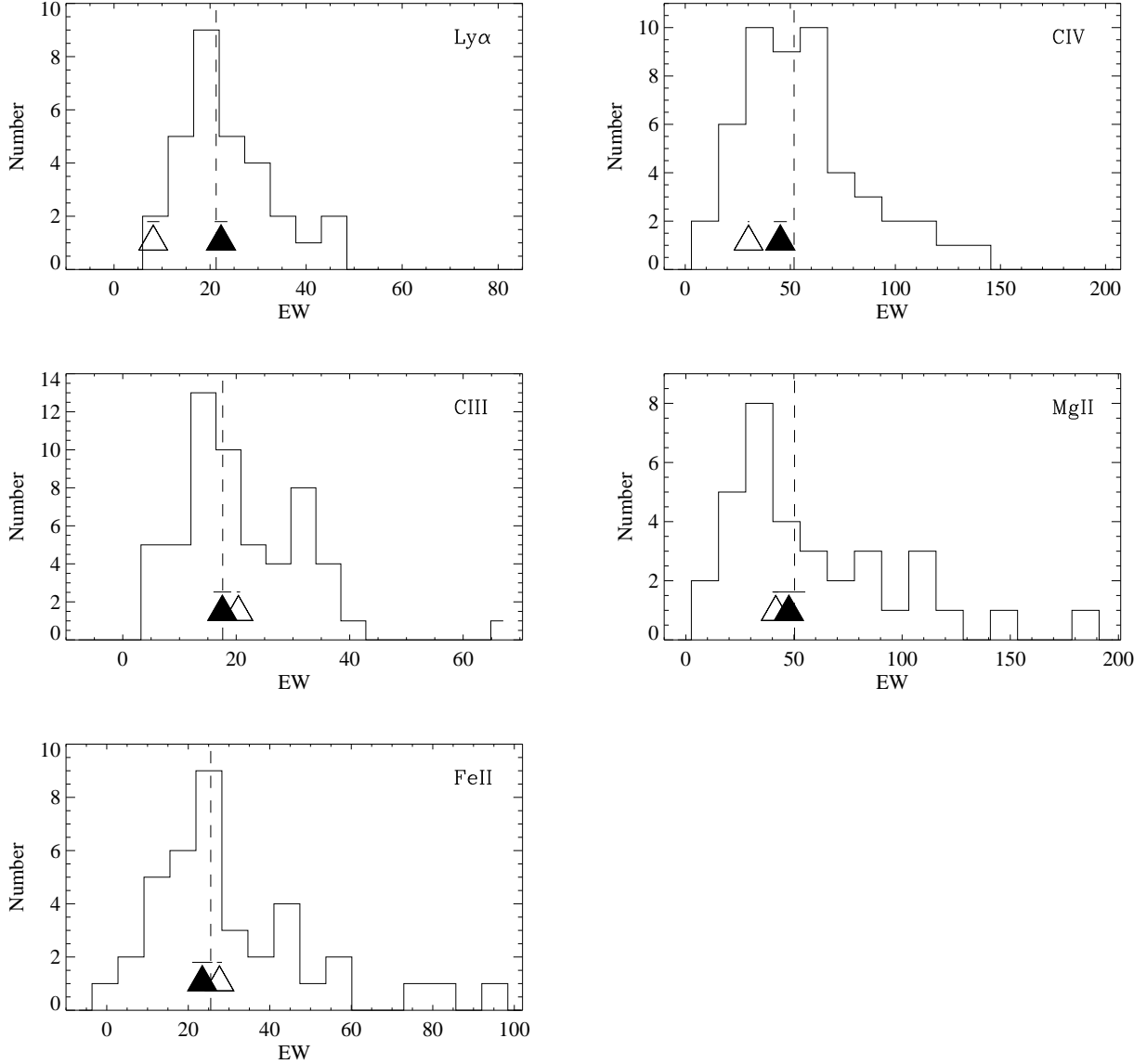


Fig. 6. Histograms of rest-frame equivalent widths measured from our PKS 0.25-0.5Jy spectra. Over-plotted are the median of the distribution (dashed line), the measurement from the PKS 0.25-0.5Jy composite spectrum (solid triangle) and the measurements from the LBQS radio-quiet composite spectrum (open triangle). The assumed error bars for the composite measurements are plotted as horizontal bars above the triangles.

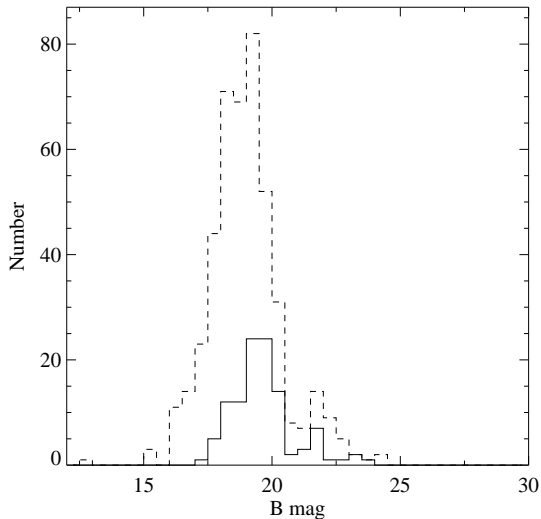


Fig. 7. Histogram of B magnitudes for all 449 quasars in the Parkes quarter-Jansky flat-spectrum sample (dashed line) and for the subset of 109 with new spectra and $0.25\text{Jy} < S_{2.7\text{GHz}} < 0.5\text{Jy}$ that were used to make the composite (solid line).

sample increases as the ratio of core-to-lobe flux (R) decreases, i.e. as the implied viewing angle to the radio jet axis increases.

The EW ratios from composite spectra given in Table 1 are relative measurements using the same method on each composite and are therefore largely independent of the details of the continuum fitting and flux integration method used to determine the EWs. The absolute EW measurements shown in Figure 6 were only used to estimate the uncertainty in the value measured from the PKS 0.25-0.5Jy composite.

We note that Francis et al. (2002) have measured rest-frame EWs from the stronger, flat spectrum radio sources ($S_{2.7\text{GHz}} \geq 0.5\text{Jy}$) in the PKS sample. We have used the electronic table from that paper to derive median EWs of 40.13 ± 3.40 , 20.61 ± 1.75 and 29.61 ± 1.13 for CIV, CIII] and MgII respectively (this combines the data from their red and blue sub-samples, which showed no significant differences in these lines). The value for CIII] is similar to ours for weaker PKS 0.25-0.5Jy radio sources, but the median values for CIV and MgII are lower than ours at the $2 - 3\sigma$ level and closer to the values we derive for the LBQS composite. However, since this comparison involves absolute EW measurements made by different groups and hence may be affected by systematic measurement effects, we do not consider the differences to be significant.

6. The Lyman- α flux decrement as a function of Redshift

Our spectra can also be used to measure the mean flux decrement shortward of the Ly α emission line as a function of redshift. We used the same method as previous authors

(e.g. Oke & Korycansky 1982, Schneider et al. 1991b), namely to calculate

$$D_A = 1 - \frac{f(\text{observed})}{f(\text{continuum})} \quad (1)$$

where $f(\text{observed})$ is the observed flux averaged over the rest-frame region $1050 - 1170\text{\AA}$ and $f(\text{continuum})$ is the expected continuum flux in the same region, which is estimated by extrapolating the continuum redward of the Ly α emission line into the blue.

There were 22 quasars in our sample for which we obtained a spectrum and which have sufficiently high redshift ($z \geq 2.4$) for the region around the Ly- α line to be covered. (Note that the full $1050-1170\text{\AA}$ region is not covered in all cases but enough of the region is covered to give a good measurement of D_A .) The D_A values are plotted against redshift for the PKS QSOs in Figure 8. For comparison, values are plotted for optically selected QSOs taken from Schneider, Schmidt and Gunn (1991a, 1991b). Also plotted are other values from the literature (Oke & Korycansky 1982, Steidel & Sargent 1987). Only optically-selected QSOs from these papers are plotted.

In the lower panel of Figure 8 the same data are plotted in bins of 0.5 in redshift. Points are plotted at the median redshift and D_A values within each bin. The errors in the median were estimated by taking the standard deviation in each bin and dividing by \sqrt{N} (the bins containing only one point have undefined error bars). The plot shows that there is no significant difference between the two sets of points. This indicates that neither sample is significantly biased towards or against QSOs with a large amount of Ly- α absorption.

7. Conclusions

We have presented spectra and redshift measurements for a large sample of radio-selected quasars which, when combined with data from the literature, forms a complete sample of radio-loud quasars. We have studied statistical properties of the new spectra, in particular the rest-frame equivalent width distribution of the rest-frame UV spectral lines and the Lyman- α decrement at high redshift. We find that the spectra we have obtained show significantly stronger Ly α and CIV emission lines than radio-quiet quasars from the LBQS, which has a similar optical magnitude distribution to our sample. We find no major difference in the Lyman- α decrement measured from our spectra compared to those of optically-selected QSOs at similar redshifts.

Acknowledgements. We are grateful to Paul Francis for generating and making available a new version of the composite spectrum of LBQS radio-quiet QSOs. We also thank the helpful support staff at the ESO 3.6m, where the majority of our spectroscopic observations were carried out. This paper has benefited from helpful comments from the referee, Dr. P. J. P. McCarthy.

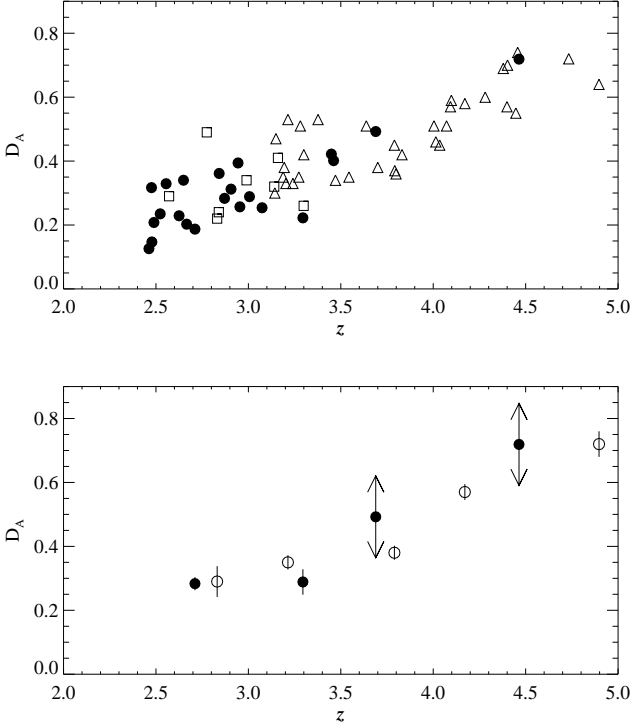


Fig. 8. Upper panel: The Lyman- α decrement D_A as a function of redshift. Filled circles represent quasars from the Parkes quarter-Jansky flat-spectrum sample, open symbols represent optically-selected QSOs from the literature. The latter points are taken from Schneider, Schmidt and Gunn (1991a, 1991b; triangles) and from Oke & Korycansky (1982) and Steidel & Sargent (1987; squares). Lower panel: The same data in bins of 0.5 in redshift, with the optically-selected samples combined. The points are plotted at the median (z, D_A) within each bin. $1\text{-}\sigma$ error bars are plotted except for cases where the bin only contains one object in which case arrows are drawn.

Appendix A: Tables

Table A.1. Redshifts for the Parkes quarter-Jansky flat-spectrum sample. An asterisk next to the name indicates a note in the text for that object. The “conf” column gives a level of confidence in the redshift (0=no lines for redshift determination, 1=secure redshift, 2=single line or weak lines). The Class column gives the classification, reproduced from Jackson et al. (2002). These classifications are based on both the spectrum and images of the source and their meanings are as follows: Q = confirmed quasar by spectroscopy or UVX photometry; BL = spectroscopically-confirmed BL Lac object; G = Galaxy with morphological or spectroscopic confirmation; NCS = Non-compact radio source (the source is either a steep-spectrum or extended radio source). Refer to individual notes in Jackson et al (2002) for full details.

Name	z	Conf	Class	Date
B0000–160	0.508	1	G	Oct 95
B0008–307	1.189	1	Q	Oct 97
B0012–184	0.743	1	Q	Oct 97
B0017–307	2.666	1	Q	Oct 97
B0022–044	1.946	1	Q	Oct 97
B0026–014	0.083	1	G	Oct 95
B0027–426	0.495	1	Q	Oct 97
B0038–326	–	0	BL	Oct 97
B0039–407*	2.478	1	Q	Oct 97
B0056–525	–	0	BL	Oct 94
B0059–287	1.694	1	Q	Oct 95
B0111–256	1.030	1	Q	Oct 97
B0113–283	2.555	1	Q	Oct 97
B0115–016	1.162	1	Q	Oct 95
B0115–342	0.647	1	Q	Oct 97
B0118–272	–	0	BL	Oct 97
B0136–059	2.004	1	Q	Oct 97
B0138–097*	–	0	BL	Oct 97
B0140–059	–	0	BL	Oct 97
B0143–061	0.499	1	NCS	Oct 95
B0144–219	0.262	1	G	Oct 94
B0150–144	1.349	1	Q	Oct 97
B0213–026	1.177	1	Q	Oct 94
B0214–085	–	0	BL	Oct 97
B0214–330	1.331	1	Q	Oct 97
B0217–189	–	0	BL	Oct 97
B0227–369	2.115	1	Q	Oct 97
B0238–052	–	0	BL	Oct 97
B0240–060	1.805	1	Q	Oct 97
B0245–167	–	0	BL	Oct 97
B0256–393	3.449	1	Q	Oct 97
B0258+011	1.221	1	Q	Oct 97
B0258–184	1.627	1	Q	Oct 97
B0258–344	1.704	1	Q	Oct 97
B0315–282	1.166	1	Q	Oct 97

Name	z	Conf	Class	Date	Name	z	Conf	Class	Date
B0323-244	1.161	1	Q	Nov 93	B1021-323	1.568	1	Q	May 97
B0334-131	1.303	1	Q	Oct 97	B1027-186	1.784	1	Q	May 97
B0341-256	1.419	1	Q	Oct 97	B1036-431	1.356	1	Q	May 97
B0346-163	–	0	BL	Oct 97	B1046-222	1.609	1	Q	May 97
B0347-211	2.944	1	Q	Nov 93	B1055-248	0.593	1	Q	May 97
B0348-326	0.927	1	G	Oct 95	B1055-301	2.523	1	Q	May 97
B0351-701	0.455	1	Q	Oct 95	B1056-113	–	0	BL	May 97
B0357-264*	–	0	BL	Nov 93	B1105-304	0.740	1	Q	May 97
B0400-319	1.288	1	Q	Nov 93	B1110-355	1.695	1	Q	May 97
B0406-056	0.304	1	G	Oct 97	B1117-270	1.881	1	Q	May 97
B0411-462	2.223	1	Q	Nov 93	B1118-140	1.114	1	Q	May 97
B0420+022	2.277	1	Q	Oct 97	B1119-069	–	0	BL	May 97
B0420-484	0.527	1	Q	Oct 95	B1133-032	1.648	1	Q	May 97
B0422-389	2.346	1	Q	Oct 97	B1136-156*	2.625	1	Q	May 97
B0426-380	–	0	BL	Oct 97	B1147-192	2.489	1	Q	May 97
B0427-435	1.423	1	Q	Oct 97	B1149-084	2.370	1	Q	May 97
B0432-440	2.649	1	Q	Oct 97	B1206-202	0.404	1	G	Apr 95
B0436-203	2.146	1	Q	Oct 95	B1206-238	1.299	1	Q	May 97
B0446-370	0.561	1	Q	Oct 97	B1210-097	–	0	BL	May 97
B0447-010	0.487	1	Q	Oct 97	B1213-102	0.636	2	Q	May 97
B0500+019	0.584	1	G	Oct 94	B1224-443	–	0	BL	Apr 95
B0524-433	2.164	1	Q	Oct 97	B1230-101	2.394	1	Q	May 97
B0534-340	0.683	1	Q	Oct 97	B1240-059	0.139	1	G	Apr 95
B0601-172	2.711	1	Q	Oct 97	B1240-394	1.387	1	Q	May 97
B0602-424	0.611	1	Q	May 97	B1241-399	0.191	1	Q	May 97
B0610-316	0.873	1	Q	May 97	B1245-062	0.762	1	Q	May 97
B0610-436	3.461	1	Q	May 97	B1248-350	0.410	1	Q	May 97
B0613-312	–	0	BL	May 97	B1250-330	0.859	2	Q	May 97
B0625-401	–	0	G	Oct 95	B1251-407*	4.464	1	Q	May 94
B0627-199	–	0	BL	Oct 94	B1256-177	1.956	1	Q	May 97
B0630-261	0.717	1	Q	May 97	B1300-105	–	0	BL	May 94
B0637-337	–	0	BL	May 97	B1319-093	1.864	1	Q	May 97
B0644-390	0.681	1	Q	May 97	B1320-338	1.346	1	Q	May 97
B0646-306*	1.153	1	Q	Nov 93	B1321-105	0.872	2	Q	May 97
B0700-465	0.822	1	Q	Nov 93	B1324-047	1.882	1	Q	May 97
B0726-476	2.282	1	Q	Nov 93	B1330-143	–	0	BL	May 97
B0806-710	0.333	1	Q	Apr 95	B1331-115	1.402	2	Q	May 97
B0834-223	0.837	1	Q	Oct 95	B1333-049	–	0	BL	Apr 95
B0907+022	–	0	BL	May 97	B1336-237	0.657	2	Q	May 97
B0913+003	3.074	1	Q	Oct 95	B1339-206	1.582	1	Q	May 97
B0930-338	0.936	1	Q	May 97	B1339-287	1.442	1	Q	May 97
B0933-333	2.906	1	Q	May 97	B1346-139	0.253	1	G	Apr 95
B1005-333	1.837	1	Q	May 97	B1348-289	1.034	2	Q	May 97
B1008+013	–	0	BL	May 97	B1354-107	3.006	1	Q	Apr 95
B1009-328	1.745	1	Q	May 97	B1358-090	0.667	1	Q	May 97
B1010-427	2.954	1	Q	May 97	B1358-298	0.689	1	Q	Apr 95
B1016-268	–	0	BL	May 97	B1412-096	2.001	1	Q	May 97
					B1415-349	1.544	1	Q	May 97

Name	z	Conf	Class	Date
B1418-064	3.689	1	Q	May 97
B1422-250	1.884	1	Q	May 97
B1427-448	–	0	BL	May 97
B1430-155	1.583	1	Q	Apr 95
B1438-328	1.479	1	Q	May 97
B1451-248	1.216	1	Q	May 97
B1452-367	0.095	1	G	Apr 95
B1454-354	1.424	1	Q	Apr 95
B1455-060	–	0	BL	Apr 95
B1519-294	2.126	1	Q	Apr 95
B1533-316	–	0	BL	May 97
B1635-035	2.871	1	Q	May 97
B1657+022	2.039	1	Q	May 97
B1701+016	2.842	1	Q	May 97
B1728+004	1.335	1	Q	May 97
B2012-017	–	0	BL	Oct 97
B2014-380	0.598	2	BL	May 97
B2053-391	1.937	1	Q	Apr 95
B2054-377	1.071	1	Q	May 97
B2110-160	1.638	1	Q	May 97
B2116-113	1.844	1	Q	Oct 97
B2123-015	2.196	1	Q	May 97
B2153-008	0.495	2	BL	May 97
B2156-203	0.057	1	NCS	Oct 95
B2217-011	1.878	1	Q	May 97
B2221-116	0.115	2	BL	May 97
B2224+006	2.248	1	Q	Oct 95
B2233-173	0.647	1	Q	May 97
B2244-002	0.094	2	G	May 97
B2245-059	3.295	1	Q	May 97
B2251+006	–	0	BL	Oct 94
B2251-419	1.765	1	Q	May 97
B2253-278	1.751	1	Q	May 97
B2254-204	–	0	BL	Oct 97
B2258-022	0.778	2	Q	Oct 97
B2303-656*	0.47	2	G	Oct 94
B2306-312	1.380	1	Q	Oct 97
B2311-373	2.476	1	Q	Oct 97
B2315-172	2.462	1	Q	Oct 97
B2315-404	1.820	1	Q	Oct 97
B2320-021	1.774	1	Q	Oct 97
B2322-482	0.221	1	BL	Nov 93
B2332-293	0.931	1	Q	Oct 97
B2333-415	1.406	1	Q	Oct 97
B2337-334	1.802	1	Q	Oct 97
B2351-309	–	0	BL	Oct 97
B2351-413	0.632	2	Q	Oct 97
B2354-021	–	0	BL	Oct 97

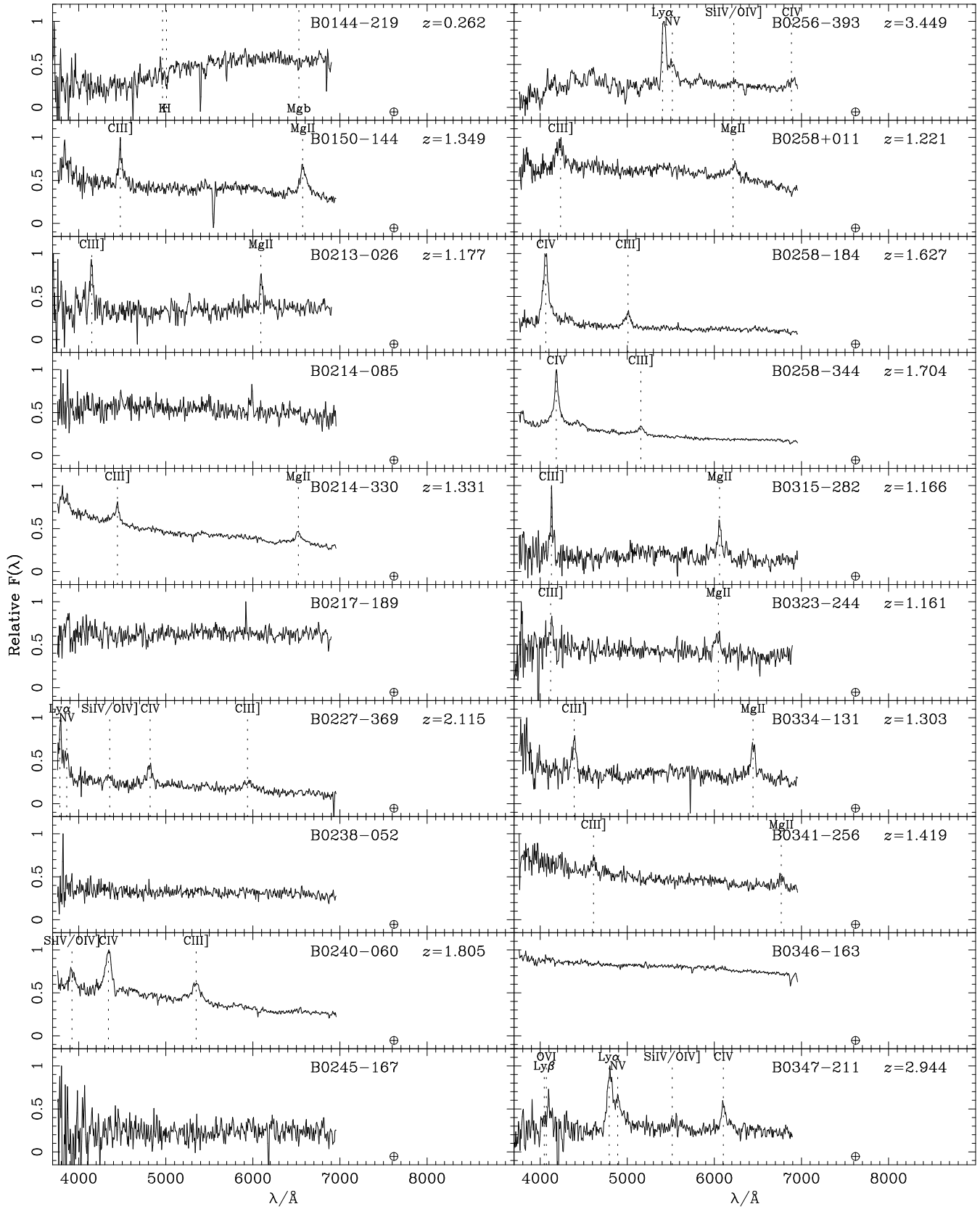


Fig. 1. continued

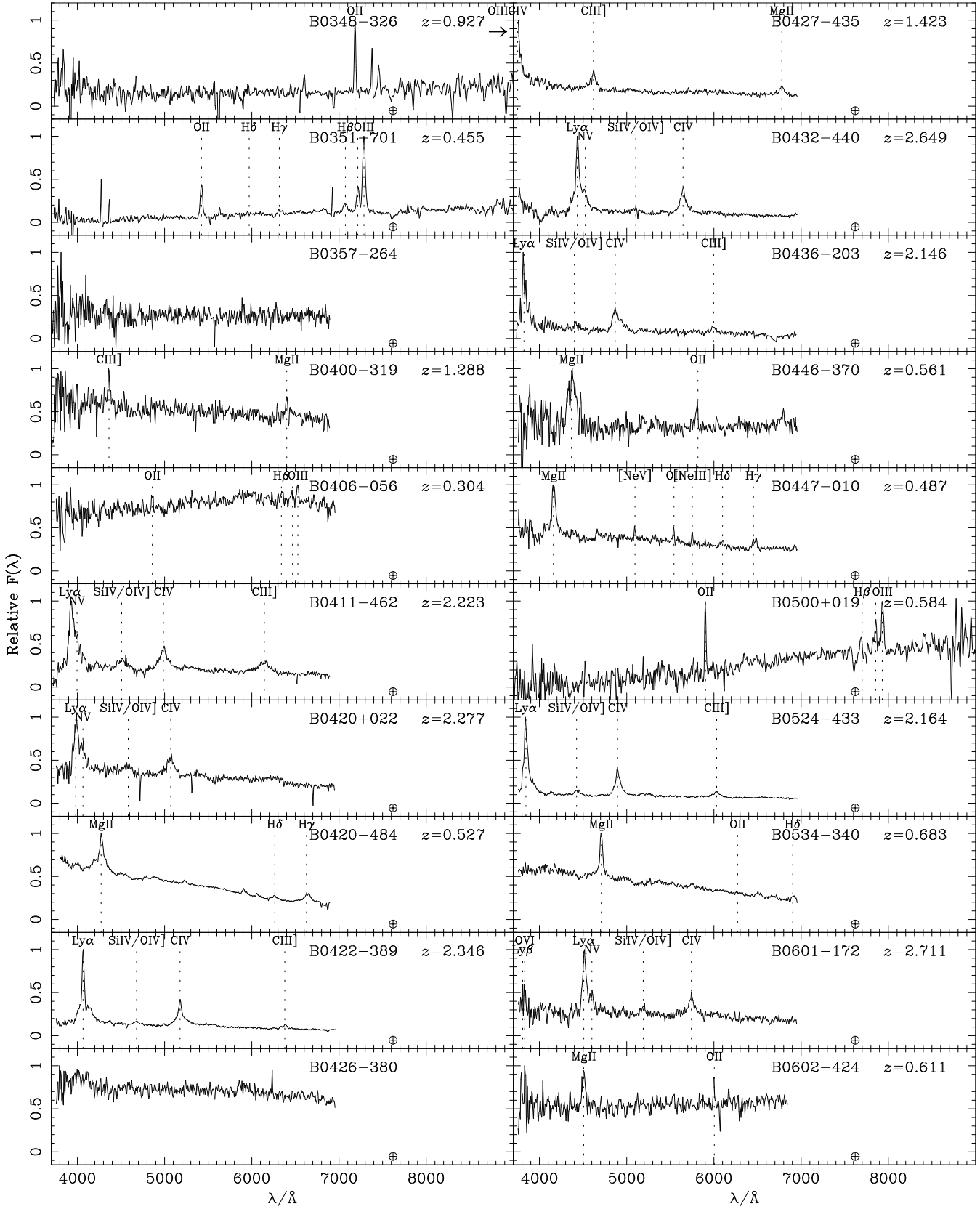


Fig. 1. continued

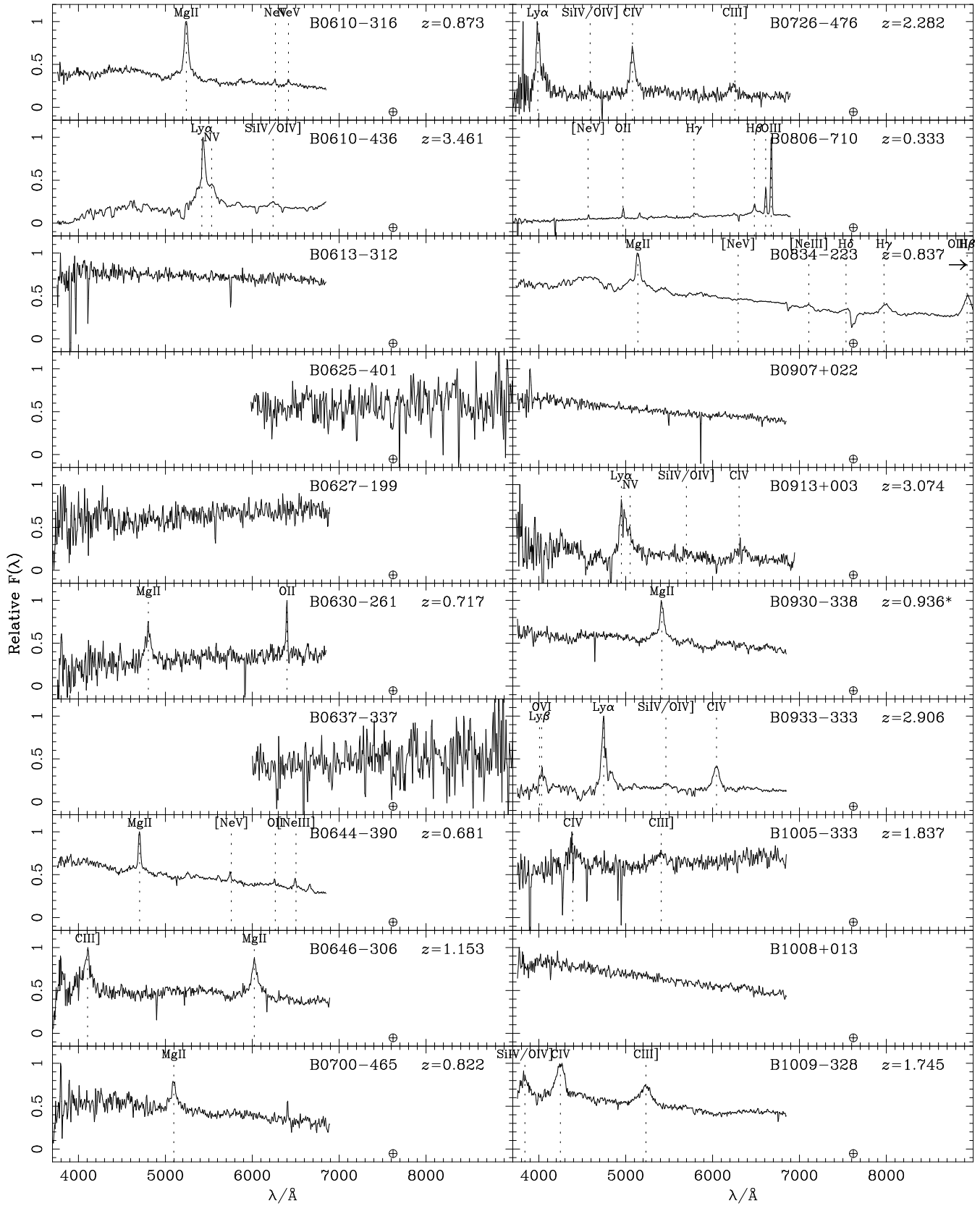


Fig. 1. continued

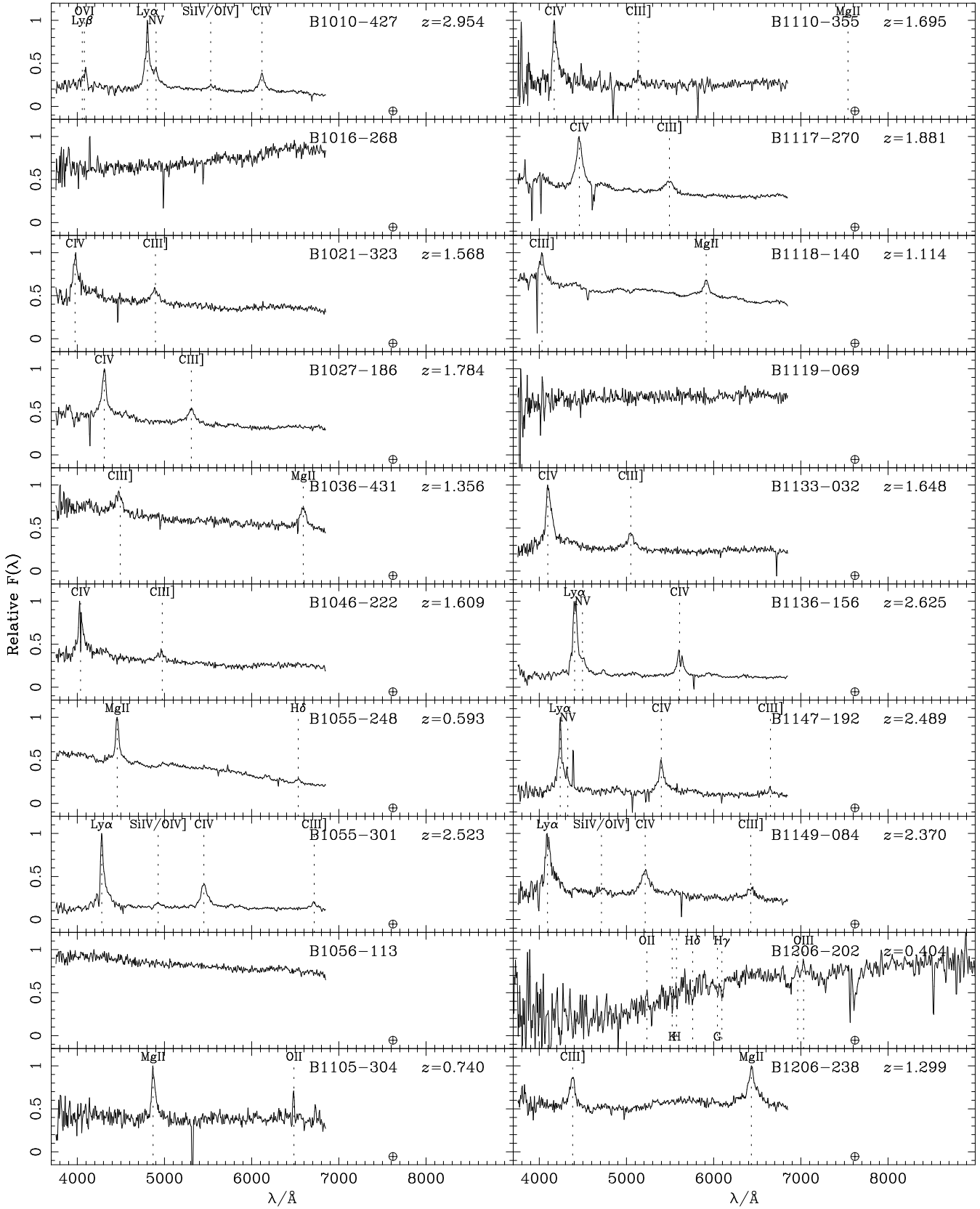


Fig. 1. continued

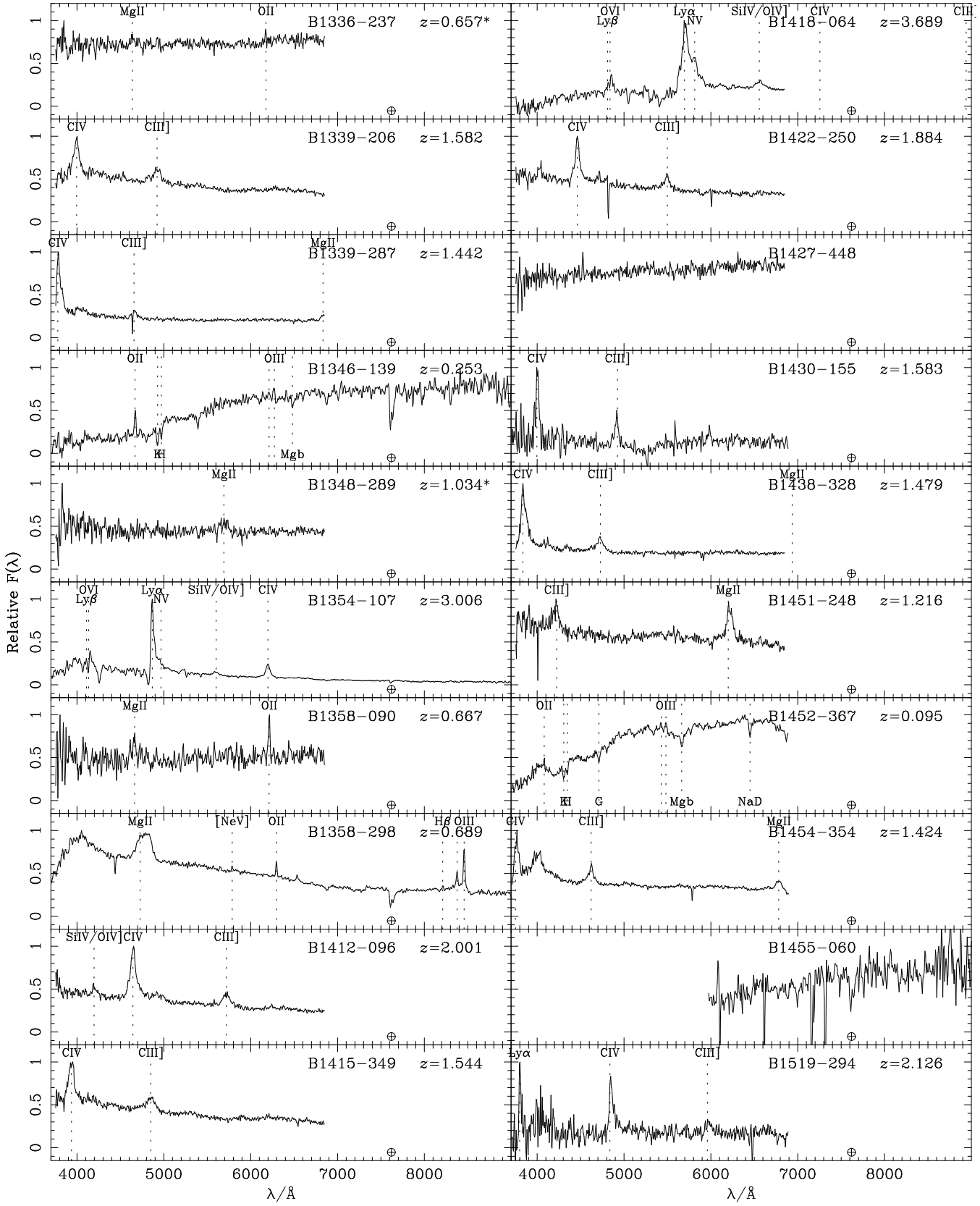


Fig. 1. continued

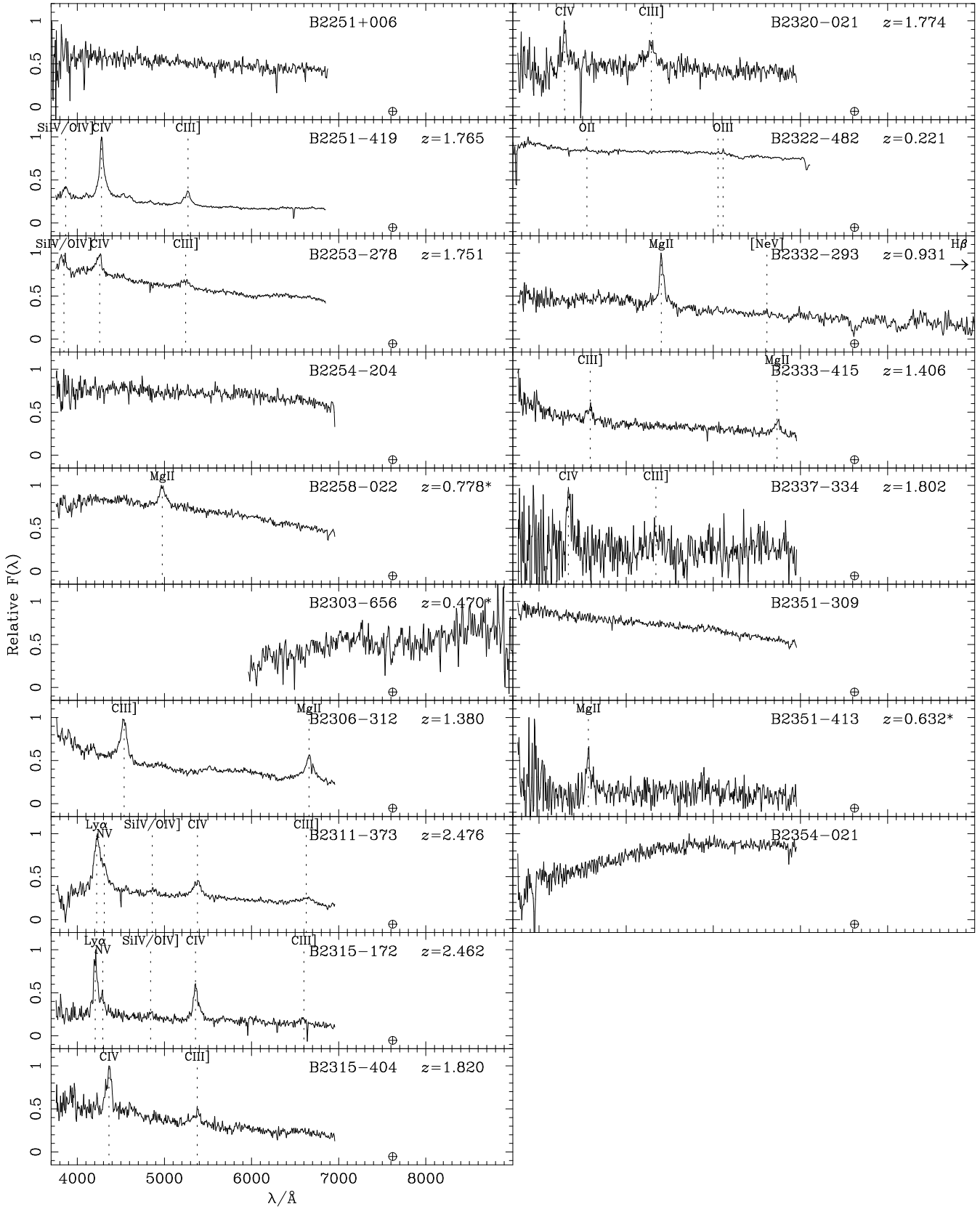


Fig. 1. continued

References

- Baker, J. C., Hunstead, R. W., ApJ, 452, L95
- Becker, R. H., White, R. L., Helfand, D. J. 1995, ApJ, 450, 559
- Brotherton, M. S., Tran, H. D., Becker, R. H., Gregg, M. D., Laurent-Muehleisen, S. A., White, R. L., 2001, ApJ, 546, 775
- Corbin, M. R., 1992, ApJ, 391, 577.
- Corbin, M. R., Francis, P. J., 1994, AJ, 108, 2016.
- Drinkwater M. J., Webster R. L., Francis P. J., Condon J. J., Ellison S. L., Jauncey D. L., Lovell J., Peterson B. A., Savage A., 1997, MNRAS, 284, 85
- Tytler D., Fan X. 1992, ApJS, 79, 1
- Ellison S. L., Yan, L., Hook I. M., Pettini M., Wall J. V., Shaver P., 2001, A&A, 379, 393
- Ellison S. L., Yan, L., Hook I. M., Pettini M., Wall J. V., Shaver P., 2002, A&A, 383, 91
- Francis P. J., Hewett, P. C., Foltz C. B., Chaffee F. H., Weymann R. J., Morris S. L., 1991, ApJ, 373, 465.
- Francis P. J., Hooper E. J., Impey C. D., AJ, 1993, 106, 417
- Francis P.J, 1993, ApJ, 405, 119
- Francis P. J., Drake C. L., Whiting M. T., Drinkwater M. J., Webster R. L., 2002, PASA, 18, 221
- Hewett, P., Foltz, C., Chaffee, F. H., 1995, AJ, 109, 149.
- Hooper E. J., Impey C. D., Foltz C. B., Hewett P. C., 1995, ApJ, 445, 62
- Iovino A., Clowes R., Shaver P. A., 1996, A&AS, 119, 265
- Jackson C. A., Wall J. V., Shaver P. A., Kellermann K. I., Hook I. M., Hawkins M. R. S., 2002, A&A, 386, 97
- McCarthy, P. J., 1993, ARAA, 31, 639
- Oke J. B., Korycansky D. G., 1982, ApJ, 255, 110
- Schneider D.P., Schmidt M., Gunn J.E., 1991a, AJ, 102, 837
- Schneider D.P., Schmidt M., Gunn J.E., 1991b, ApJ, 101, 2004
- Shaver P. A., Wall J. V., Kellermann K., 1996a, MNRAS, 278, 11L
- Shaver P. A., Wall J. V., Kellermann K. I., Jackson C. A., Hawkins M. R. S., 1996b, Nat, 384, 439
- Steidel C.C., Sargent L.W., 1987, ApJ, 313, 171
- Stoeckle J. T., Rector T. A., 1997, ApJ, 489, 17L.
- Veron-Cetty M.-P., Veron P., ESO Sci. Rep., 13, 1 (1993)
- Wall J. V., Peacock, J. A. 1985, MNRAS, 216, 173
- Wall J. V. et al 2002, in preparation